6th AIAA Flow Control Conference
25 - 28 June 2012, New Orleans, Louisiana

AIAA 2012-2681

Low Reynolds Number Stall Suppression with Dynamic Roughness

Travis Grager,[1] Alric Rothmayer,[2] Wade W. Huebsch[3], and Hui Hu[4](✉)
Department of Aerospace Engineering, Iowa State University, Ames, IA 50011

An experimental study was conducted to investigate the use of dynamic roughness to suppress stall on a NACA 0012 airfoil. Particle image velocimetry (PIV) data shows the ability of the dynamic roughness to maintain predominantly attached flow at higher angles of attack than can be reached when the dynamic roughness is not actuated. The influences of Reynolds number, roughness frequency, and roughness amplitude/height on the ability of dynamic roughness to control separation are examined.

Nomenclature

AR	=	aspect ratio (b/c)
α	=	angle of attack relative to free stream
b	=	span length
c	=	chord length
Re_c	=	chord Reynolds number
T.K.E.	=	normalized turbulent kinetic energy
$\|V\|$	=	normalized ensemble average velocity magnitude
x	=	direction aligned with the flow originated at the model leading edge
y	=	direction perpendicular to x originated at the model leading edge

I. Introduction

Low Reynolds number airfoil aerodynamics has been an area of great interest as micro aerial vehicles (MAV) have been viewed as a useful next generation of unmanned aerial vehicles (UAV). The small size of these vehicles along with their slow airspeeds places them in the low Reynolds number regime of 10^4-10^5.[1] For flows with Reynolds number at this scale and smaller, the physics are very different than those of higher Reynolds number flows associated with traditional manned aircraft. One of the predominant characteristics of this flow regime is the formation of separation bubbles at relatively low angles of attack.

Many studies have addressed airfoil aerodynamics at low Reynolds numbers along with the relationship between laminar boundary layer flow separation and the chord Reynolds number, see Tani[1], Carmichael[2], Lissaman[3], Mueller[4], and Gad-el-Hak[5], for example. According to Lissaman[3], a separation bubble occurs when the boundary layer detaches from the surface of the airfoil and then reattaches further downstream as a turbulent boundary layer. The bubble size is predominantly influenced by the Reynolds number of the flow. Initially, a separation bubble can be relatively short, but any small disturbance such as an increase of the angle of attack can cause the bubble to burst and cover much of the upper surface of an airfoil resulting in a sudden stall and loss of performance. For chord Reynolds numbers below 5.0×10^4, the chord is too short for the separated boundary layer to reattach. At a chord Reynolds number of approximately 7.0×10^4, the chord is long enough for the separated boundary layer to reattach and form the leading edge separation bubble. Above a chord Reynolds number of 1.0×10^5, the bubble length is approximately 30-40% of the chord length. In general, the separation bubble's length is inversely proportional to the Reynolds number, its thickness is proportional to its length, and the location of the laminar boundary layer separation is primarily determined by the angle of attack, and to a lesser extent by the Reynolds number. Flow measurements of laminar separation bubbles have been performed using a variety of techniques, including point wise measurements using laser Doppler velocimetry[6-8] and spatially resolved measurements such as PIV[9-12].

[1] Senior Research Engineer, Physical Science Inc., Andover, MA 01810, tgrager@psicorp.com, AIAA Member.
[2] Professor, Aerospace Engineering, AIAA Associate Fellow, Email: roth@iastate.edu.
[3] Associate Professor, Mechanical and Aerospace Engineering, West Virginia University, AIAA Senior Member.
[4] Associate Professor, Aerospace Engineering, AIAA Associate Fellow, Email: huhui@iastate.edu

In addition, many studies have experimented with different methods to control the separation bubble and increase the angle of attack at which an airfoil will stall in this low Reynolds number regime. Most of the methods have examined ways to turbulate the boundary layer. Some of these methods include: suction or injection of air into the boundary layer, static surface roughness, vibrating the surface, heating or cooling of the surface, and the use of micro-electro-mechanical systems. Rinoie et al.[13] suggested the use of a bubble burst control plate for the suppression of an airfoil stall. Their study found that attaching a stationary small plate near the leading edge of a low Reynolds number airfoil could suppress stall and increase the lift performance by preventing the small separation bubble from bursting and forming a large separation bubble. An unsteady version of the burst plate was examined by Grager et al.[14] and was also found to suppress separation.

Other studies by Huebsch[15], Honsaker & Huebsch[16], Gall et al.[17], and Huebsch et al.[18] examined the control of leading edge separation bubbles using dynamic roughness. Dynamic roughness is distributed vibrating surface roughness. In previous studies, the dynamic roughness oscillates at high frequency, has a diameter that is close to the local boundary layer thickness, and is usually shallow (with heights less than or equal to the boundary layer thickness). These studies used both two-dimensional and three-dimensional CFD simulations to show the effectiveness of dynamic roughness in suppressing a leading edge separation bubble. Along with the simulations, Gall et al.[17] and Huebsch et al.[18] used experimental smoke visualization to demonstrate the ability of dynamic roughness to suppress the leading edge separation bubble on a NACA0012 airfoil. Key findings from the Gall et al.[17] and Huebsch et al.[18] studies are that: the separation bubble can be suppressed by dynamic roughness with heights that are as small as a few percent of the boundary layer thickness, providing that the frequency is large enough (a result that is consistent with a laminar flow control mechanism suggested by Rothmayer & Huebsch[19]), the dynamic roughness affects the flow similarly to static roughness when the frequency is too low, and the dynamic roughness field does not need to start before the leading edge separation point to be able to eliminate the separation bubble. This paper extends the work of Huebsch et al.[18] by performing further experimental studies on dynamic roughness through the use of PIV.

II. Experimental Setup

This experimental study was conducted in a closed-circuit wind tunnel located in the Aerospace Engineering Department of Iowa State University. The tunnel is capable of wind speeds up to 150 mph and has a test section that has a 12 x 12 inch (304 x 304 mm) cross section with transparent walls. Installed ahead of the test section are a series of screens and a honeycomb structure followed by a contraction section which help provide uniform, low turbulence flow to the test section. The standard deviation of velocity fluctuations for the incoming flow was found to be 0.8% of the free stream velocity as measured by a hotwire anemometer.

The model tested was a straight, non-twisted wing with a NACA 0012 airfoil profile. The chord was c = 150 mm and the span b = 300 mm which resulted in an aspect ratio AR = 2. The incoming air velocity was set to 2.7, 5.3, 7.8, and 10.4 m/s which resulted in chord Reynolds numbers (Re_c) of 2.5 x 10^4, 4.9 x 10^4, 7.3 x 10^4, and 9.7 x 10^4, respectively.

The model (Figs. 1 and 2) was designed using a 3D CAD program and printed using the Objet Alaris 3D printer. The printer's extremely high accuracy, fine resolution, and very thin layer thickness (28 microns) provide for an accurate model. The model was printed in three main sections: a leading edge dynamic roughness section, an outer section that the leading edge mounts to, and the tunnel mounting section.

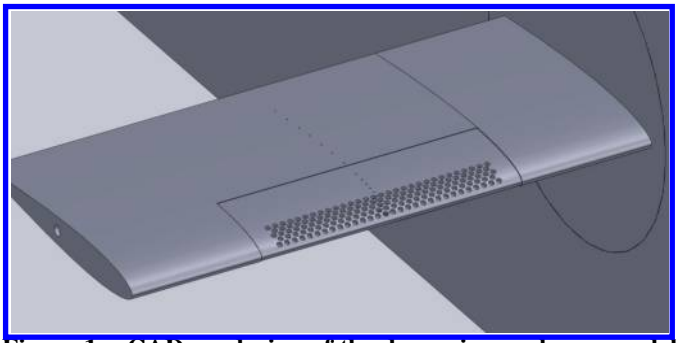

Figure 1: CAD rendering of the dynamic roughness model

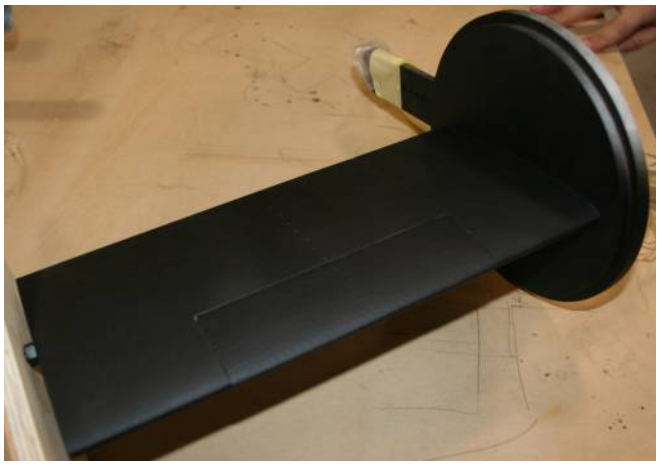

Figure 2: Finished dynamic roughness model

The leading edge dynamic roughness section has a span that is half that of the entire model and has a width of 30% chord. Attached over the entire surface of the dynamic roughness section is a thin layer (.006 in) of latex rubber that is painted with a black rubber plastic for PIV measurements, as shown in Fig. 2. This section was printed in one piece so that the inside of the model could be a hollow airtight chamber with holes only where the dynamic roughness elements are located. With latex covering these holes, when the chamber is pressurized the latex forms small round bumps on the surface, creating the roughness elements. Cycles of pressurizing and depressurizing the chamber cause the roughness elements to form and flatten, thereby creating dynamic roughness. The dynamic roughness region starts at 1.07% chord and ends at 10.76% chord. The roughness elements (example shown in Fig. 3) are 2% chord (3 mm) diameter at the base and a max height of 0.15% chord (230 microns). The 3mm diameter was taken from Huebsch et al.[18] (in fact, the airfloil, dynamic roughness placement and flow conditions are intended to reproduce the design of Huebsch et al.[18]). The quoted heights (for example, 230 microns) are the typical maximum observed heights during the oscillation (or during a static pressurization). The actual amplitudes of oscillation are considerably less than this value (typically about 25% of the maximum height). It should be noted that no attempt has been made to more accurately quantify these heights. This maximum height produces a shallow dynamic roughness field whose roughness height is expected to be considerably less that the observed boundary layer thickness (for example, about 2mm as observed from PIV measurements for Re=73,000 at 15 degrees angle of attack). This produces a dynamic roughness maximum height that is roughly 25% of the boundary layer thickness. While conditions can change considerably from case to case, we believe that the dynamic roughness used in this study is likely to lie well within the boundary layer. Elements are arranged so that they are spaced 1.46 diameters center-to-center in the spanwise direction and aligned in the streamwise direction in such a manner that the front edge of a row of elements aligns with the back edge of the elements in front of it. Rows of elements are positioned in an alternating pattern as shown in Fig. 3.

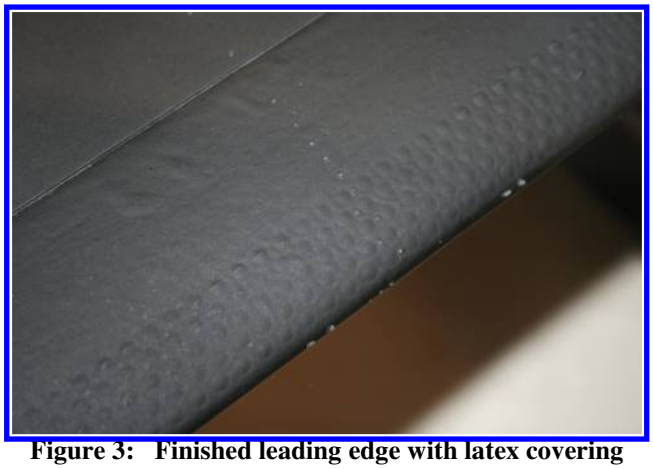

Figure 3: Finished leading edge with latex covering

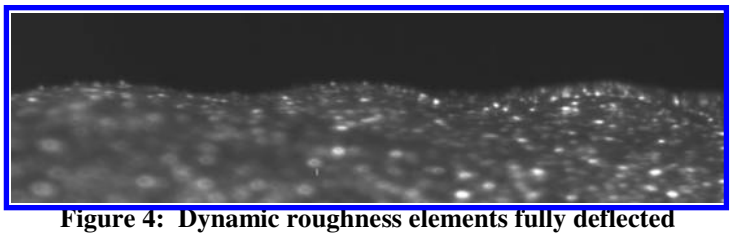

Figure 4: Dynamic roughness elements fully deflected

The air chamber beneath the dynamic roughness and within the leading edge of the airfoil was pressurized and depressurized through the use of a pump created using COTS (commercial off the shelf) parts. This system is shown in Fig. 5. A two cycle 90 cubic centimeter remote control aircraft engine served as a pump while a ½ horsepower variable speed electric motor was used to drive the aircraft engine. A set of pulleys and a belt were used to connect the motor to the engine. Copper pipe fittings were attached to the head of the motor. These fittings allowed the pressure supplied to the model to be crudely controlled through the use of a needle valve, which siphons off some of the air before it reaches the hose that is attached to the model. Controlling the pressure allows control of the maximum height of the roughness elements. A laser tachometer was used to verify the drive frequency of the engine, which was controlled to the nearest 0.5 Hz. The system was able to produce pumping frequencies up to 92 Hz. Heights were estimated from video images of the oscillating surface, such as shown in Fig. 4.

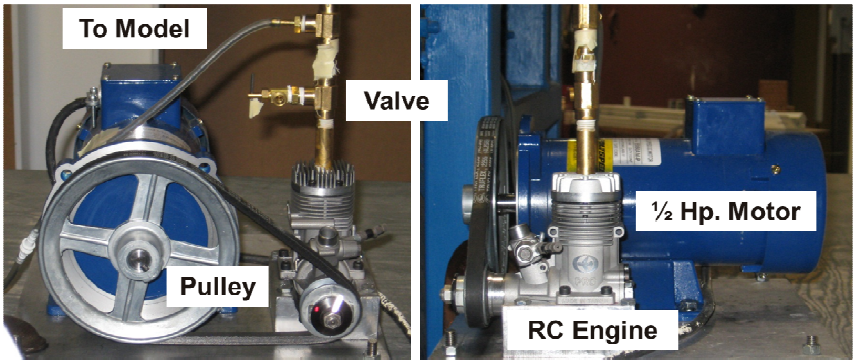

Figure 5: Actuation pump system

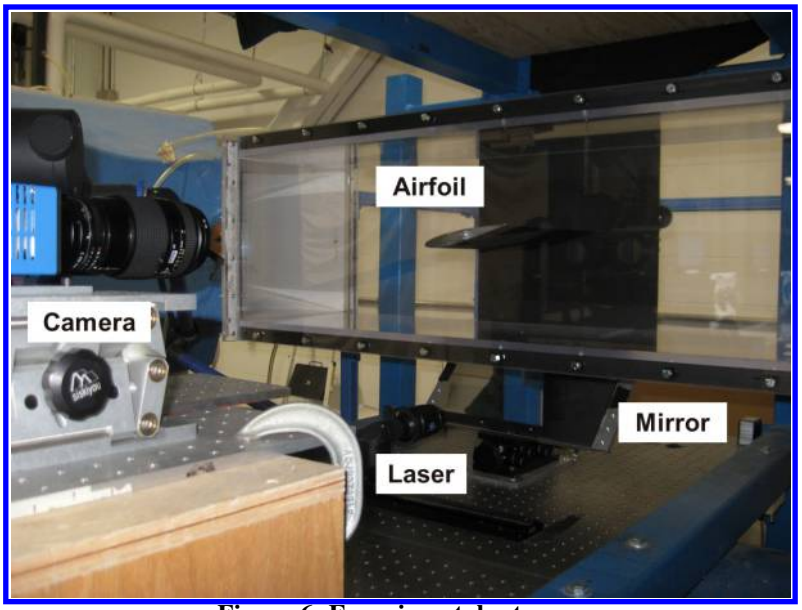

Figure 6: Experimental set-up

The experimental set-up is shown in Fig. 6. The dynamic roughness model was mounted inverted to allow easy set-up of the laser for PIV data to be taken. Two CCD cameras (Fig. 6) were used to take 2D PIV with one being used for a view of the entire airfoil and the other zoomed in on the leading edge. Both cameras were 1600 x 1200 resolution CCD cameras (PCO 1600, Cooke Corp). The flow was seeded with 1~5 micron oil droplets while illumination was provided by a double-pulsed Nd:YAG laser (NewWave Research Solo) adjusted on the second harmonic and emitting two laser pulses at a wavelength of 532 nm at a repetition rate of 3 Hz. The laser sheet was positioned and created by passing the laser beam through a laser arm and cylindrical lens and then aligned with a mirror. The laser sheet was positioned near the center span of the model and had a thickness of approximately 2 mm. The triggering of the laser and camera was controlled via a digital delay generator (Berkeley Nucleonics, Model 565). Most averaged PIV data shown in this study were based on 345 image pairs, but for those involving turbulent kinetic energy and vorticity, 900 image pairs were used.

A Reynolds number study was conducted in which the incoming flow was set to 4 different speeds (2.7, 5.3, 7.8, and 10.4 m/s) resulting in chord Reynolds numbers of 25,000, 49,000, 73,000, and 97,000, respectively.

A frequency study was conducted at an angle of attack of 14 degrees for a Reynolds number of 49,000. The pressure provided to the chamber was set to the highest possible pressure, which produced element heights of 195 micons when run at a frequency of 30 Hz, 230 microns when run at a frequency above 60 Hz, and heights between 195 and 230 microns between 30 and 60 Hz. The drive frequency was adjusted in 10 Hz increments down from 90 Hz until control was lost.

A combined height and frequency study was conducted at an angle of attack of 15 degrees for a Reynolds number of 73,000. Three frequencies (90, 60, and 30 Hz) were used, and the pressure supplied to the chamber was adjusted to obtain different roughness element heights. Due to the fact that the chamber pressure was controlled by both the release valve and the drive frequency, it was difficult to obtain the same heights for each frequency, but enough were obtained to determine how decreasing element height affects the flow control.

III. Experimental Results and Discussion

A. Reynolds Number Study

Results from the Reynolds number study are shown in Figures 7-10. These contours of average velocity, as well as arrows showing the average flow direction, clearly show the ability of dynamic roughness to control flow separation in the low Reynolds number regime. Figures 7, 8, and 10 each start at the angle where the flow starts to separate without the dynamic roughness actuated and stop at the angle where dynamic roughness no longer can control the flow well enough for complete attachment. Figure 9 starts at an angle of attack higher than the angle of attack where the flow initially starts to separate. In each figure, the left images have the dynamic roughness turned off (Clean) and the right images have the dynamic roughness turned on (DR On) with an actuation frequency of 90 Hz and a roughness height of 230 microns. Preliminary numerical and computational results (see Huebsch et al.[18]) have shown that larger element heights (as long as it is less than the boundary layer thickness) and higher actuation frequencies are more likely to control the flow; thus, it was decided to use the largest drive frequency and largest roughness height possible.

For the lowest Reynolds number case of 25,000 (Fig. 7), the flow is able to increase the angle of attack approximately 2 degrees, from 10 degrees to 12 degrees, before the airfoil stalls. Even when the airfoil is in a deep stall at 12 degrees, the dynamic roughness is able to thin the separation region in the vicinity of the leading edge. The stalling of the airfoil at this condition appears to be somewhat similar to that of a thin airfoil stall.

Approximately doubling the Reynolds number to 49,000 (Fig. 8) shows that the use of dynamic roughness increases the angle of attack range for attached flow by 3 degrees, from 13 to 16 degrees, before the airfoil goes into a deep stall. At an angle of attack of 15 degrees, the dynamic roughness is still able to control the flow across the upper surface of the airfoil, but a leading edge separation bubble is present. For angles of attack below this value, the flow is completely attached, and above 15 degrees the bubble bursts causing complete separation.

At Reynolds numbers of 73,000 and 97,000 (Figs. 9 and 10 respectively), the dynamic roughness is able to increase the angle of attack range of completely attached flow by about 3 degrees as well, but from 14 to 16 degrees as opposed to 13 to 15 degrees for the Re = 49,000 case. Comparing the two higher speed cases, they both have

relatively large separation bubbles at 16 degrees, but the lower speed case (Fig. 9) has a thicker bubble. At 17 degrees, the lower Reynolds number case is in fully developed deep stall while the higher Reynolds number case has a very large separation bubble covering a distance of more than half the airfoil. Any slight disturbances will burst this bubble which makes it a very unstable flow condition.

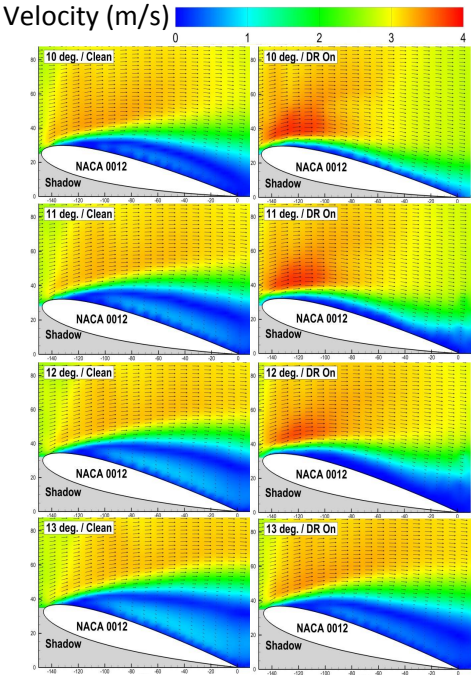

Figure 7: Average velocity contours, Re_c = 25,000

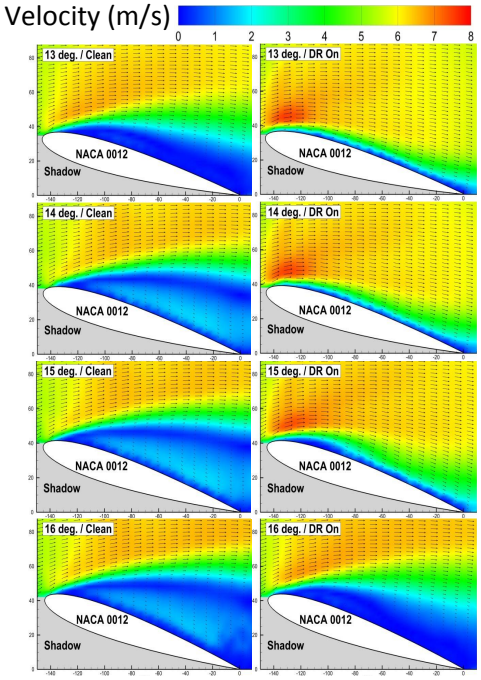

Figure 8: Average velocity contours, Re_c = 49,000

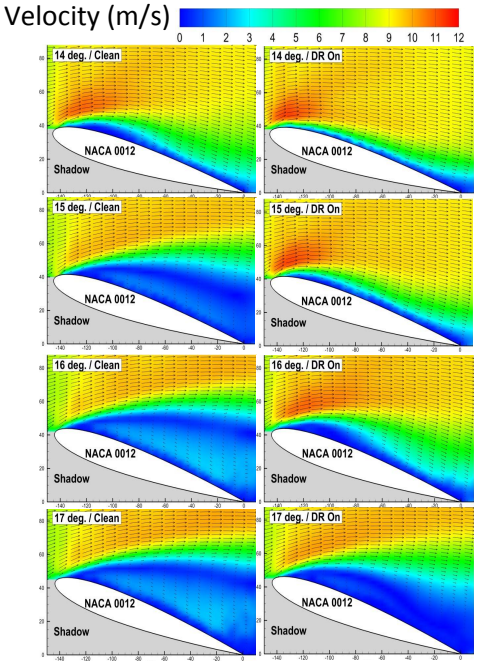

Figure 9: Average velocity contours, Re_c = 73,000

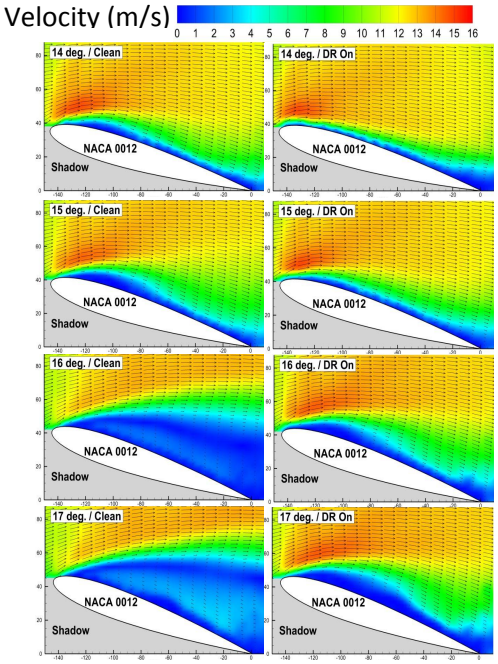

Figure 10: Average velocity contours, Re_c = 97,000

In general, while within the low Reynolds number regime, the higher the Reynolds number, the higher the angle of attack at which a separation bubble will appear when the dynamic roughness is turned on. The higher the Reynolds number, the smaller the separation bubble and the easier it is control the flow. These results have shown that at Reynolds numbers on the order of 50,000 to 100,000, dynamic roughness can generally increase the stall angle of a NACA 0012 airfoil by about 2 to 3 degrees.

B. Frequency Study

Results from the frequency study are shown in Figures 11 and 12 with the first figure showing the average velocity contours on the upper surface of the entire airfoil and the second zoomed in on the leading edge. From these figures and at this set of flow conditions (Reynolds number = 49,000 and angle of attack = 14 degrees), it can be seen that the airfoil is in a fully developed deep stall without the dynamic roughness actuating. Once the roughness is actuated at or above a frequency of 50 Hz, the flow becomes reattached to the leading edge of the upper surface bringing the airfoil out of stall. At actuation frequencies at or below 40 Hz, the flow becomes separated putting the airfoil back into a stall. This observed frequency toggle is consistent with the results of Huebsch[15], Honsaker & Huebsch[16], Gall et al.[17], and Huebsch et al.[18].

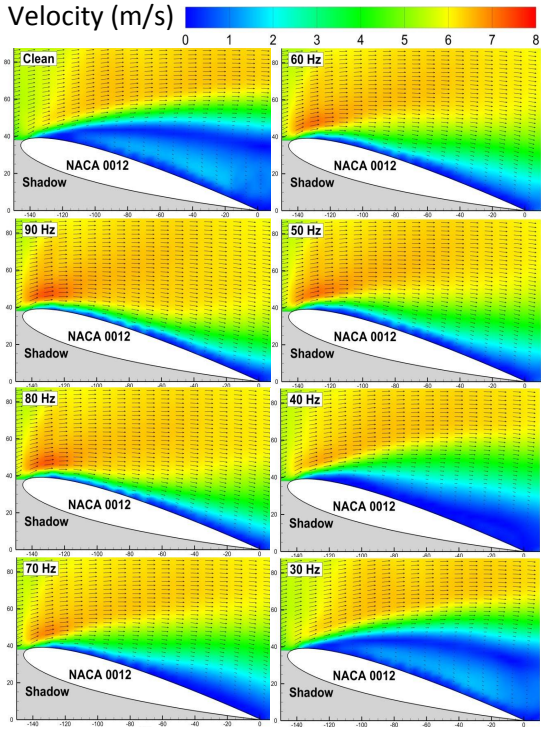

Figure 11: Average velocity contours (wide view) for different dynamic roughness control frequencies.
Angle of attack = 14°, Re_c = 49,000

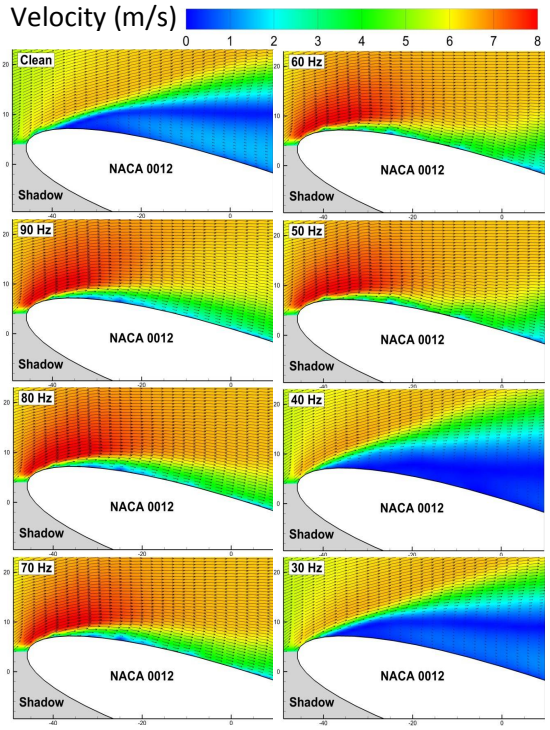

Figure 12: Average velocity contours (zoom view) for different dynamic roughness control frequencies.
Angle of attack = 14°, Re_c = 49,000

Examples of the averaged vorticity in Figs. 13 and 14, as well as turbulent kinetic energy (TKE) in Figs. 15 and 16, were obtained as part of the frequency study. It should be noted that TKE is defined in the usual manner, but no distinction has been made between turbulent flow and forced unsteady flow. For vorticity and TKE, both the clean airfoil and the highest frequency case are shown. From the vorticity images in Figs. 13 and 14, it can be seen that when the flow is not controlled there is a shear layer separating from the leading edge. When the dynamic roughness is engaged, the boundary layer is kept attached to the leading edge. In both Figs. 13 and 14, the detached

region of large vorticity is pulled onto the surface. The wide view of Fig. 13 suggests that the region of large vorticity thickens near the leading edge and may extend slightly further downstream when the dynamic roughness is turned on. However, the close up of the leading edge (Fig. 14) shows that the region of high vorticity right at the nose of the airfoil when the dynamic roughness is turned on is either the same as or slightly thinner than the vorticity layer thickness for a clean airfoil. There appears to be some thickening of the high vorticity region in the lower Fig. 14 just downstream of the leading edge and this is consistent with the thickening of the high vorticity region seen in Fig. 13. The streamwise extent of the high vorticity region in Fig. 14 is definitely smaller when the dynamic roughness is turned on. It is possible that some of the differences between the plots may be due to the differences in the scales used for the vorticity. Simply based on observations of averaged vorticity, it is not possible to determine whether or not the dynamic roughness is significantly changing the overall level of vorticity.

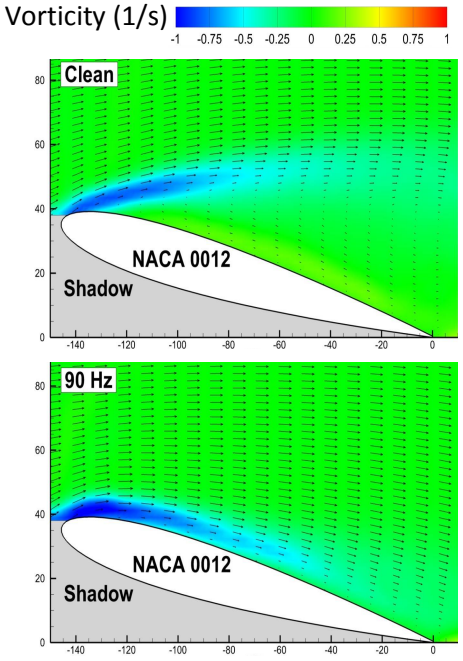

Figure 13: Average vorticity contours for uncontrolled (clean) and controlled (90 Hz, 230 micron dynamic roughness) wide view
Angle of attack = 14°, Re_c = 49,000

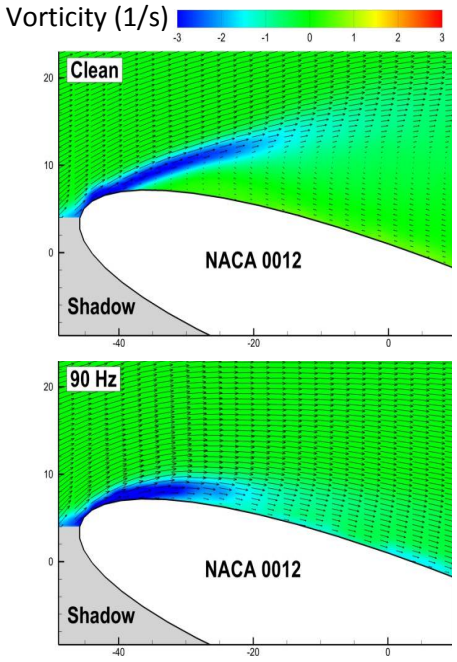

Figure 14: Average vorticity contours for uncontrolled (clean) and controlled (90 Hz, 230 micron dynamic roughness) zoom view
Angle of attack = 14°, Re_c = 49,000

The TKE contours of Figs. 15 and 16 show that when the flow is separated from the airfoil with the dynamic roughness turned off (the top figures of Figs. 15 and 16), there is a large amount of TKE in the wake region of the airfoil that emanates from the detached shear layer, as expected, with very little TKE near the leading edge. With the dynamic roughness actuated (the bottom figures of Figs. 15 and 16) there is an increased amount of TKE generated near the leading edge. In particular, there is a large amount of turbulence directly above and behind the dynamic roughness region (i.e. the orange region in the lower figure of Fig. 16) which is likely assisting in reattaching the flow. This region of enhanced TKE may be responsible for the thickening of the vorticity layer near the leading edge of the airfoil observed in Figs. 13 and 14. The turbulence dissipates further downstream of the dynamic roughness region, but reappears closer to the trailing edge. When dynamic roughness reattaches the flow at the leading edge in Figs. 15 and 16, the airfoil begins to stall from the trailing edge. The trailing edge separation is likely to be causing the high levels of turbulence near the trailing edge for the attached case.

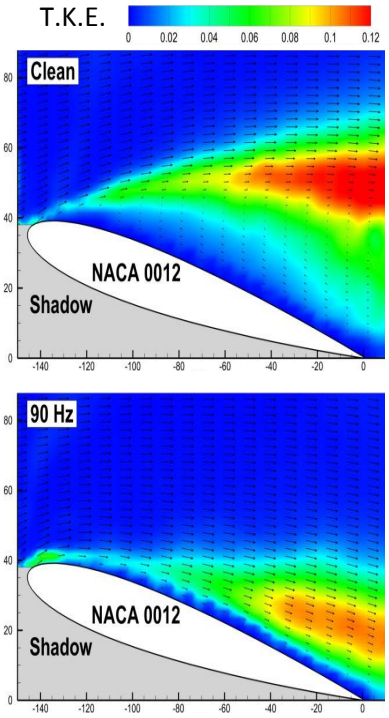

Figure 15: Turbulent kinetic energy contours for uncontrolled (clean) and controlled (90 Hz, 230 micron dynamic roughness) wide view
Angle of attack = 14°, Re_c = 49,000

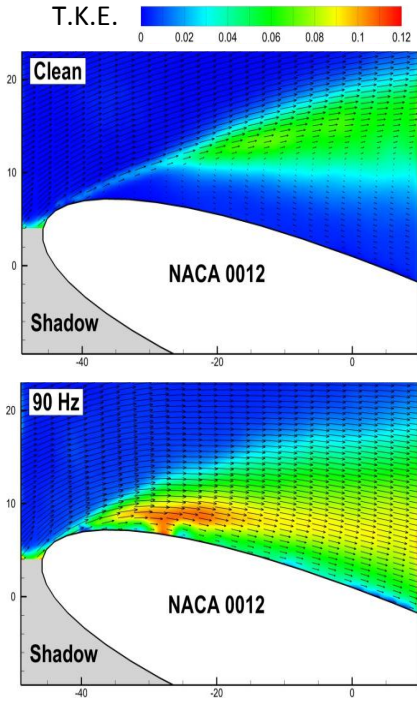

Figure 16: Turbulent kinetic energy contours for uncontrolled (clean) and controlled (90 Hz, 230 micron dynamic roughness) zoom view
Angle of attack = 14°, Re_c = 49,000

C. Roughness Height Study

The results of the roughness height study are shown in Figure 17. Due to the difficulties in obtaining the same roughness heights at all frequencies, only a select number of roughness heights and frequencies were chosen to demonstrate the effect of roughness element height on flow control. The frequency and height for each case are shown in the upper left corner of each image.

The flow is attached to the airfoil for dynamic roughness running at 90 Hz and the largest element height that could be produced, i.e. 230 microns. Reducing the roughness height to 105 microns at that frequency results in the formation of a leading edge separation bubble. Reducing the frequency to 60 Hz and increasing the roughness element height back to 230 microns also results in a leading edge separation bubble. Maintaining the frequency at 60 Hz and reducing the element height to 80 and 60 microns slightly increases the size of the leading edge separation bubble.

Further reduction in the dynamic roughness actuation frequency to 30 Hz while maintaining element heights of 80 and 60 microns substantially deteriorates the flow control. The 30 Hz, 80 micron case is slightly worse than the 60 Hz, 60 micron case, but once the roughness height is decreased to 60 microns at 30 Hz then all flow control is lost and the airfoil goes into a deep stall. For the cases considered in this study, increasing the dynamic roughness amplitude and frequency improves flow control. This observation is consistent with previous results by Huebsch[15], Honsaker & Huebsch[16], Gall et al.[17], and Huebsch et al.[18].

It should be noted that the only case in Fig. 17 that has reasonably full control of the separation is the 90 Hz, 230 micron case. Likewise, there is also only one case that is fully stalled, i.e. the 30 Hz, 60 micron case. There are a wide range of cases (i.e. all cases except the 90 Hz, 230 micron and 30 Hz, 60 micron cases) where there is partial control of separation (in the sense that the deep stall region has been substantially reduced but there is still some separation present on the airfoil). In the partially controlled cases of Fig. 17, the size of the separation does not change that much from case to case. The CFD results of Huebsch et al.[18] also produce a range of cases with partial control, at lower frequencies and roughness heights. Full control was not observed by Huebsch et al.[18] unless a combination of height and frequency exceeded a large critical value.

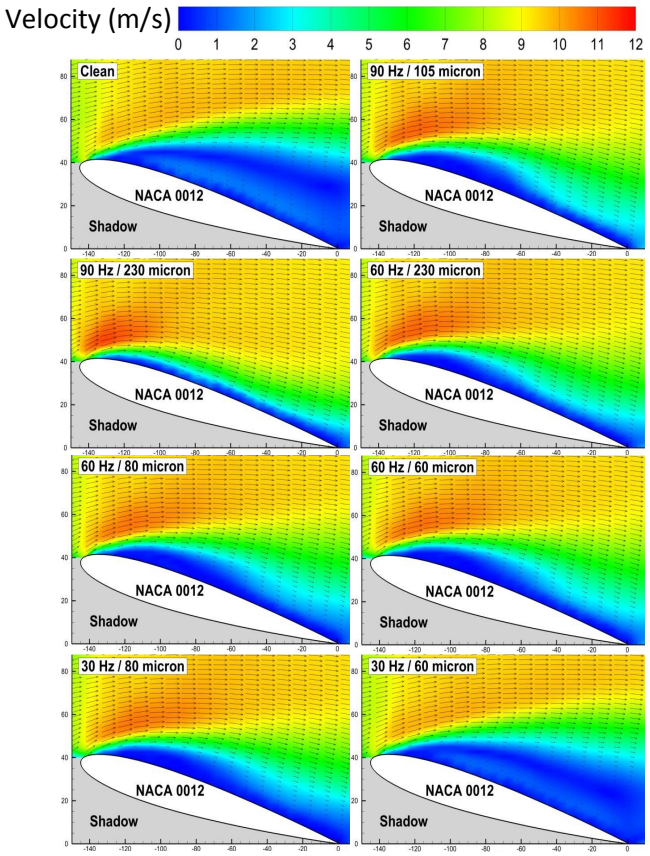

Figure 17: Average velocity contours for roughness element height and frequency study
Angle of attack = 15^o, Re_c = 73,000

III. Conclusion

An experimental investigation was conducted to assess the performance of dynamic roughness as a flow control device for airfoil separation at low Reynolds numbers. At low frequencies, the dynamic roughness does not affect stall. However, above a threshold frequency the dynamic roughness is found to suppress stall and produce a predominantly attached flow, providing that the angle of attack is not too large (a result that is consistent with previous studies). Dynamic roughness was found to suppress deep stall for about 2-3 degrees above the angle of attack where the clean airfoil stalls. This is in contrast to previous work, which only considered the suppression of a small leading-edge separation bubble. For the dynamic roughness considered in this study, it was found that increasing the roughness amplitude and frequency improved the flow control (a result that is also consistent with previous studies). Even at the relatively low (30-90 Hz, maximum) frequencies used in this study, dynamic roughness can significantly increase the angle at which an airfoil will stall. Further research is needed to quantify how much more lift can be generated as dynamic roughness frequency is increased, as well as the power requirements needed to operate a dynamic roughness device.

Acknowledgments

The authors would like to thank William Rickard and James Benson of the Iowa State University WiST (Wind Simulation and Testing) Laboratory as well as the members of Advanced Flow and Experimental Aerodynamics Laboratory for their help and support in conducting this study. The authors would also like to thank Richard Guiler at Physical Sciences Inc. (PSI) for his helpful suggestions and comments throughout the course of this study. This research was partially sponsored by the U.S. Air Force and Physical Sciences Inc., and this study does not necessarily reflect the position or the policy of the Government or PSI and no official endorsement is or should be inferred.

References

[1]Tani, I., 1964, "Low Speed Flows Involving Bubble Separations," *Prog. Aeronaut. Sci.*, Vol. 5, pp. 70–103.

[2]Carmichael, B. H., 1981, "Low Reynolds Number Airfoil Survey," *NASA CR-165803*, Vol. 1.

[3]Lissaman, P. B. S., 1983, "Low-Reynolds-Number Airfoils," *Annual Review of Fluid Mechanics*, Vol. 15, pp.223–239.

[4]Mueller, J. T., ed., 2001, "Fixed and Flapping Wing Aerodynamics for Micro Air Vehicle Applications," *Progress in Astronautics and Aeronautics*, Vol. 195, AIAA.

[5]Gad-el-Hak, M. 2001, "Micro-Air-Vehicles: Can They be Controlled Better," *Journal of Aircraft*, Vol. 38, No. 3, pp. 419-429.

[6]FItzgerald, E. J., and Mueller, T. J., 1990, "Measurements in a Separation Bubble on an Airfoil Using Laser Velocimetry," AIAA J., 28_4_, pp. 584–592.

[7]Brendel, M., and Mueller, T. J., 1987, "Boundary Layer Measurements on an Airfoil at Low Reynolds Numbers," AIAA Paper No. 87-0495.

[8]O'Meara, M. M., and Mueller, T. J., 1987, "Laminar Separation Bubble Characteristics on an Airfoil at Low Reynolds Numbers," AIAA J., 25_8_, pp. 1033–1041.

[9]Lang, M., Rist, U., and Wagner, S., 2004, "Investigations on Controlled Transition Development in a Laminar Separation Bubble by Means of LDA and PIV," *Exp. Fluids*, 36, pp. 43–52.

[10]Ol, M. V., Hanff, E., McAuliffe, B., Scholz, U., and Kaehler, C., 2005, "Comparison of Laminar Separation Bubble Measurements on a Low Reynolds Number Airfoil in Three Facilities," 35th AIAA Fluid Dynamics Conference and Exhibit, Toronto, Ontario, June 6–9, AIAA Paper 2005-5149.

[11]Raffel, M., Favier, D., Berton, E., Rondot, C., Nsimba, M., and Geissler, M., 2006, "Micro-PIV and ELDVWind Tunnel Investigations of the Laminar Separation Bubble Above a Helicopter Blade Tip," *Meas. Sci. Technol*., 17, pp. 1652–1658.

[12]Burgmann, S., Brücker, S., Schröder, W., 2006, "Scanning PIV Measurements of a Laminar Separation Bubble," *Exp. Fluids*, 41, pp. 319–326.

[13]Rinoie, K., Okuno, M., and Sunada, Y., 2009, "Airfoil Stall Suppression by Use of a Bubble Burst Control Plate", AIAA Journal Vol. 47, No. 2, Feb. 2009.

[14]Grager, T., Rothmayer, A. P., and Hu, H., 2011, "Low Reynolds Number Stall Suppression with Dynamic Burst Control Plate," AIAA Paper 2011-1180, presented at the 49th Aerospace Sciences Meeting, Orlando FL, Jan. 4-7, 2011.

[15]Huebsch, W. W., 2004, "Dynamic Surface Roughness for Aerodynamic Flow Control," AIAA Paper 2004-587, presented at the 42nd AIAA Aerospace Sciences Meeting and Exhibit, January 5-8 2004, Reno, Nevada.

[16]Honsaker, R., and Huebsch, W. W., 2005, "Parametric Study of Dynamic Surface Roughness as a Mechanism for Flow Control," AIAA Paper 2005-4732, 23rd AIAA Applied Aerodynamics Conference 6-9 June 2005, Toronto, Ontario Canada.

[17]Gall, P. D., Huebsch, W. W., and Rothmayer, A. P., 2010, "Dynamic Roughness as a Means of Leading-Edge Separation Flow Control," *27th International Congress of the Aeronautical Sciences.*

[18]Huebsch, W. W., Gall, P. D., Hamburg, S. D., and Rothmayer, A. P., 2012, "Dynamic Roughness as a Means of Leading-Edge Separation Flow Control," *J. Aircraft*, Vol. 49, No. 1, pp. 108-115 (January-February 2012).

[19]Rothmayer, A. P., and Huebsch, W. W., 2011, "On the Modification of Laminar Boundary Layers Using Unsteady Surface Actuation," AIAA Paper 2011-4016, presented at the 6th AIAA Theoretical Fluid Mechanics Conference, Honolulu, HW, June 2011.